Scaling theory for the statistics of slip at frictional interfaces

T. W. J. de Geus and Matthieu Wyart
Physics Institute, École Polytechnique Fédérale de Lausanne (EPFL), CH-1015 Lausanne, Switzerland

(Received 26 April 2022; revised 12 September 2022; accepted 7 October 2022; published 8 December 2022)

Slip at a frictional interface occurs via intermittent events. Understanding how these events are nucleated, can propagate, or stop spontaneously remains a challenge, central to earthquake science and tribology. In the absence of disorder, rate-and-state approaches predict a diverging nucleation length at some stress σ^*, beyond which cracks can propagate. Here we argue for a flat interface that disorder is a relevant perturbation to this description. We justify why the distribution of slip contains two parts: a power law corresponding to "avalanches" and a "narrow" distribution of system-spanning "fracture" events. We derive novel scaling relations for avalanches, including a relation between the stress drop and the spatial extension of a slip event. We compute the cut-off length beyond which avalanches cannot be stopped by disorder, leading to a system-spanning fracture, and successfully test these predictions in a minimal model of frictional interfaces.

DOI: 10.1103/PhysRevE.106.065001

I. INTRODUCTION

When a frictional interface is driven quasistatically, periods of loading are punctuated by sudden macroscopic slip events. Field observations on earthquakes [1,2] and laboratory studies support that slip nucleates at weak regions of the interface and then propagates ballistically as a fracture [3–11]. Understanding under which conditions large slip events are triggered and can propagate is central to tribology, for example, to explain the observed variability of friction coefficients [12–14]. It is also key for earthquake science [15]. Earthquakes are power-law distributed when averaged over many faults [16]. When fault specific data are considered, observations are debated. Some studies find a bimodal distribution, consisting of a power-law behavior at small magnitude on several decades, an absence of events at intermediate magnitude, and a few top outliers for which the magnitude is large [17]. Other studies suggest instead a continuous power law [18]. This debate is complicated by the fact that an individual fault consists of many segments, whose length distribution is itself self-similar [19]. Here we propose an explanation for the bimodal distribution of slip events when slip occurs at a single interface, which we consider to be disordered but essentially flat.

These questions are complicated by the fact that frictional forces can decrease with sliding velocity. Various mechanisms can lead to such a velocity weakening, including thermal creep [20–25] or the mere effect of inertia [26–29]. Rate-and-state models [2,30–32] describe the dynamics of frictional interfaces via differential equations that capture velocity weakening. The latter is characterized by a length scale L_c below which its effect is small in comparison to elastic forces [33–38]. Importantly, in the case where the stress as a function sliding velocity displays a minimum $\sigma_{\min}$, this approach predicts [8,39,40] a characteristic stress σ^* very close to $\sigma_{\min}$, beyond which a slip pulse of spatial extension larger than L^* will invade the system. In Ref. [40], it is found that $L^*/L_c \sim (\sigma - \sigma^*)^{-1}$. Yet these results apply when the interface is homogeneous: Their validity in the presence of disorder nor their connection to the observed broad distribution of earthquakes is clear.

Another approach describes how an elastic manifold driven through a disordered medium can be pinned by disorder [41,42] and was specifically applied to frictional interfaces [26,27,41,42]. In simple settings that exclude the existence of velocity weakening, the stress of a quasistatically driven interface converges to some critical value, where slip events are power-law distributed. Unfortunately, these results do not apply in presence of velocity-weakening effects where even the presence of large *avalanches*[1] was debated [26,43–45], yet experimentally observed in Ref. [46]. Very recently [47], we introduced a minimal model of frictional interfaces that contains long-range elastic interactions, disorder, and inertia. Criticality was observed, with power-law avalanches whose size can span four decades as the stress reaches some critical value σ_c. Yet inertia introduces novel phenomena. For example, in a finite system the distribution of events is bimodal: Power-law-distributed avalanches coexist with system-spanning events. Which mechanism causes such large avalanches, and how their duration, length scale, and stress drop are related to each other remain unknown, as is the relationship between σ_c governing avalanches and rate-and-state approaches.

In this article, we argue theoretically that $\sigma_c = \sigma^*$, implying that rate-and-state approaches capture the critical stress affecting the slip statistics. Yet, we find that disorder is a relevant perturbation: Consequently, previous results for the diverging nucleation length scale near σ_c neither based on

[1]In this article we define *avalanches* as a cascade of slip events that does not involve the entire system.

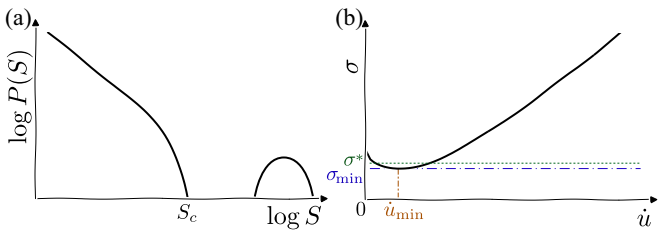

FIG. 1. (a) Sketch of distribution of avalanche sizes in a finite system: On the left there is a power-law distribution cut-off beyond some characteristic value S_c, and on the right there are system-spanning events. (b) Sketch of a flow curve (stress σ vs slip rate $\dot{u}$) with a minimum at $\sigma = \sigma_{\min}$ (with corresponding slip rate $\dot{u}_{\min}$).

a homogeneous system [40] nor on Griffith's argument [47] apply. Our current analysis justifies the presence of large power-law avalanches and leads to scaling relations between their length, stress drop, and duration, which are found to be related to a fractal property of the slip geometry at the interface. We successfully test all predictions numerically in the minimal model proposed in Ref. [47].

II. SCALING THEORY FOR SLIP EVENTS WITH VELOCITY WEAKENING

A. Observables describing slip events

We characterize slip events by their linear spatial extension (or "width" in one dimension) A, the total slip (the increment of slip, or increment of displacement discontinuity, integrated across the event's "width") S, and their duration T. As sketched in Fig. 1(a) and as reported in some systems displaying stick-slip [17,28,47], the distribution $P(S)$ consists of two parts. First, there is a power-law distribution cut-off beyond some characteristic value S_c, i.e., $P_a(S) = S^{-\tau} f(S/S_c)$ where f is a rapidly decreasing function of its argument. We call the associated events ($S < S_c$) "avalanches" and denote by A_c their cut-off spatial extension along the interface. Second, there are system-spanning slip events of extension $A \approx L$, where L is the system size, resulting in the "bump" at large S in Fig. 1(a). Empirical observations [48,49] support the existence of scaling behaviors for avalanches:

$$P(S) \sim S^{-\tau}, \tag{1}$$

$$S \sim A^{d_f}, \tag{2}$$

$$T \sim A^{z}. \tag{3}$$

A fourth scaling relation was instead observed in the simple model of a frictional interface of Ref. [47]:

$$A_c \sim (\sigma - \sigma_c)^{-\nu}. \tag{4}$$

B. Observables describing the static interface

We consider an interface that is overall flat and homogeneously loaded. Disorder can be exogenous, stemming for example from asperities on the surfaces of the two bodies, or instead be endogenous and result from the history from previous slip events that lead to irregular stresses along the interface. On loading, the interface will acquire some slip $u(r)$ at location r. Due to the disorder, $u(r)$ will fluctuate spatially. These fluctuations can be characterized by introducing the roughness exponent ζ of the interface [42]:

$$||u(r) - u(r')|| \sim ||r - r'||^{\zeta} \tag{5}$$

with $||\dots||$ the root-mean-square.

We have so far introduced five exponents: τ, ζ, ν, z, and d_f. Our central goal is to propose three new scaling relations relating ζ, ν, z, and d_f together, allowing for a stringent empirical test of our views.

C. Effect of disorder on the rate-and-state description

Previous attempts to describe the joint effects of disorder and velocity weakening sought to treat the latter as a perturbation [26,43]. We take the opposite approach, and seek to characterize how disorder affects the dynamics of a homogeneous interface subjected to velocity weakening, as captured by the rate-and-state description [8,40]. The relationship $\sigma(\dot{u})$ between the far-field stress σ and the slip rate $\dot{u}$, at any location, is key in this approach. If it does display a minimum $\sigma_{\min}$ for some slip rate $\dot{u}_{\min}$ as illustrated in Fig. 1(b), then it was shown that beyond some stress σ^* just above $\sigma_{\min}$, slip events of length $L^* \sim (\sigma - \sigma^*)^{-1}$ can nucleate system-spanning events [40].

However, where it makes sense for a homogeneous system to consider σ^* as a quantity that does not vary in space, in a disordered system its structure is locally random. A patch of material of linear extension A can still be described by some effective threshold $\sigma^*(A)$, but this quantity must vary in space. $\sigma^*(A)$ thus display fluctuations, whose magnitude we denote $\delta\sigma^*(A)$. They can only disappear in the thermodynamic limit $A \to \infty$ where randomness self-averages and homogenization is achieved. In general one expects:

$$\delta\sigma^* \sim A^{-\chi}. \tag{6}$$

Classical arguments based on disorder imply $\chi \leqslant (d + \zeta)/2$ [42,50].[2] Here d is the dimension of the interface (separating objects of dimensions $d + 1$). Below we will provide data supporting that this bound is not saturated.

If $\chi \leqslant 1$ (as we shall confirm empirically for $d = 1$), we now argue that due to these fluctuations, rate-and-state results on nucleation in homogeneous systems cannot apply to disordered ones. Indeed, consider $\sigma - \sigma^*$ to be small but positive, and a slip event occurring on a length scale $L^* \sim (\sigma - \sigma^*)^{-1}$. On that length scale, the fluctuations of σ^* are stronger than the distance to threshold $\sigma - \sigma^*$ when the latter is small: $\delta\sigma^*(L^*) \sim (L^*)^{-\chi} \sim (\sigma - \sigma^*)^{\chi} \gtrsim (\sigma - \sigma^*)$. Thus this theory neglecting the fluctuations of σ^* cannot self-consistently hold near threshold.

[2]When a portion of linear length A of the interface moves, it will explore a new realization of the disorder. If the disorder is assumed to have no spatial correlations, then that motion will be affected by $N_r = \mathcal{O}(S)$ random numbers, where S is the integrated slip. We shall see below that S follows $S \sim A^{d+\zeta}$. From the central limit theorem, any threshold characterizing motion cannot be defined with a precision finer than $1/\sqrt{N_r}$, leading to the bound stated in the main text.

D. Roughness of the interface

As discussed above, the strength $\sigma^*(A)$ of a patch of size A varies in space. The interface must adjust to these variations: The slip $u(r)$ will be larger at locations r where $\sigma^*(A)$ is small. Fluctuations of elastic stresses follow fluctuations of strain, which between two points r and r' are of order $||u(r) - u(r')||/||r - r'||$. If $||r - r'|| \sim A$, then, using Eq. (5), these fluctuations are of order $A^{\zeta-1}$. As is more generally the case for an elastic manifold in disordered environments [42], we expect such adjustments of the interface slip to stop when these fluctuations of elastic stresses are of order of the fluctuations of $\sigma^*(A)$ on that scale [of order $A^{-\chi}$, see Eq. (6)], leading to:

$$\chi = 1 - \zeta. \tag{7}$$

E. Justifying power-law avalanches

We now argue that Eq. (6) gives a natural explanation for the presence of power-law slip events or 'avalanches'. Consider a system at $\sigma = \sigma^*$ where a slip starts to occur at the origin, whose extension grows in time as $A(t)$. During this process, the system encounters new realizations of the disorder and also explores larger regions of space. Thus, the effective threshold $\sigma^*[A(t)]$ for slip propagation felt on that scale will vary in time. The dynamics will stop if it becomes larger than the applied stress, i.e., $\sigma^*[A(t)] > \sigma^* = \sigma$.

Following the depinning literature, simple arguments then constrain the statistics of stopping events [42]. $\sigma^*[A(t)]$ can be thought as a random variable that evolves continuously around its mean σ^*. $\sigma^*[A(t)]$ will lose memory of its current value when the patch size $A(t)$ increases significantly, i.e., $\sigma^*[A(t_1)]$ at time $t_1 > t_0$ decorrelates from $\sigma^*[A(t_0)]$ when $A(t_1) - A(t_0) \geqslant A(t_0)$. As a result, every time A doubles in size, there is a finite probability p_2 that $\sigma^*[A(t)] - \sigma^*$ has changed sign, and that slip has stopped. Such a property implies a power-law distribution $P(A) \sim A^{-\tau_A}$ with $\tau_A = 1 - \ln(1 - p_2)/\ln(2)$.[3] Thus we predict that the stress σ_c at which avalanches are power law, follows:

$$\sigma_c = \sigma^*. \tag{8}$$

F. Maximal avalanche extension A_c

Consider the same argument applied to the case $\sigma > \sigma^*$. As long as the scale of fluctuations $\delta\sigma^*(A) \gg \sigma - \sigma^*$, the difference $\sigma - \sigma^*$ is insignificant (as sketched in Fig. 2), and one recovers a power-law distribution of slip events as argued above. However, in the other limit where $\delta\sigma^*(A) \ll \sigma - \sigma^*$, one always has $\sigma^*(A) < \sigma$. In that regime, disorder cannot stop a propagating "crack": disorder is irrelevant, and the interface can be safely approximated to be homogeneous. Rupture is then predicted to be correctly described by homogeneous rate-and-state laws.

The crossover between these two regimes occurs for a slip extension A_c satisfying $\delta\sigma^*(A_c) \sim \sigma - \sigma^*$. Using Eqs. (6) and (5) one obtains $A_c \sim (\sigma - \sigma_c)^{-\nu}$ [Eq. (4)] with:

$$\nu = \frac{1}{\chi} = \frac{1}{1 - \zeta}, \tag{9}$$

which corrects a Griffith argument proposing $\nu = 2$ [47], which neglected the (dominant) effect of disorder.

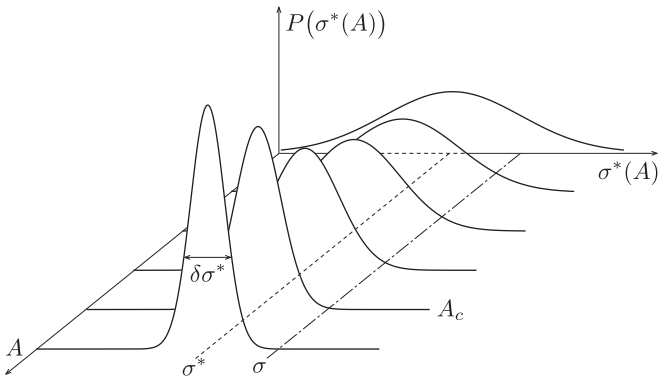

FIG. 2. (Sketch) A patch of size A has a strength $\sigma^*(A)$, which, due to disorder, is distributed around its thermodynamic value σ^*. Denoting $\delta\sigma^*(A)$ the width of this distribution for a given size A, $\delta\sigma^*$ will decrease as A increases—a large patch has a better estimate of the true, thermodynamic, σ^*. Consequently, if an event is nucleated at $\sigma > \sigma^*$, then disorder can still stop the event if its width A is sufficiently small [$\delta\sigma^*$ is large for small A, so there is a finite probability that for that region in space $\sigma^*(A) > \sigma$]. However, an event of size $A > A_c$ cannot be stopped by disorder, as the probability that that region in space has a strength $\sigma^*(A) > \sigma$ vanishes.

G. Geometry of avalanches

When slip occurs on a length scale A, the disorder characterizing this region evolves. Locally, the interface strength can decrease by some increment $\delta\sigma^*(A) \sim A^{-\chi}$. Slip will stop when the local stress, proportional to u/A, decreases by a similar magnitude. It corresponds to a slip of order u satisfying $u/A \sim A^{-\chi}$. Using that by definition $S \sim A^d u$ then leads to $S \sim A^{d_f}$ [Eq. (2)] with:

$$d_f = d + 1 - \chi = d + \zeta. \tag{10}$$

Note that Eqs. (7), (9), and (10) are well known to hold in the absence of inertia and velocity weakening [42]. The proposition that they describe the pinning of velocity-weakening elastic materials, where avalanches coexist with system-spanning events and where the flow curve has a minimum at finite slip rate, is to the best of our knowledge new. Indeed, most previous theoretical works argued that power-law avalanches would be absent in that case [26,43]. Yet the values of the exponents will differ in the absence or presence of large inertia, as we document below. We now turn to a scaling relation that is specific to the presence of velocity weakening.

H. Duration of avalanches

For stresses in the vicinity of σ^*, according to the flow curve sketched in Fig. 1(b), slip is possible only if the slip rate lies in the vicinity of $\dot{u}_{\min}$. We make the hypothesis that within

[3] Such a property reads $[\phi(A) - \phi(2A)]/\phi(A) = p_2$, where $\phi(A)$ is the cumulative distribution characterizing the probability that slip is larger than A, $\phi(A) = \int_{y>A} dy[P(y)] \sim A^{1-\tau_A}$.

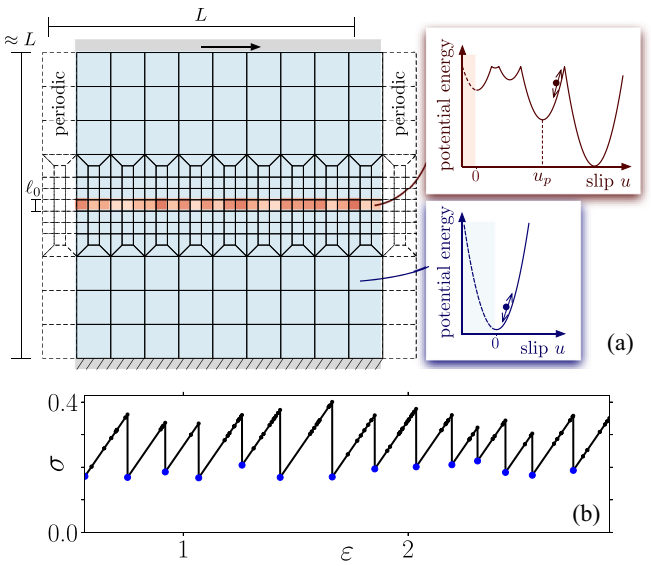

FIG. 3. (a) The frictional interface is modelled using L "blocks" (finite elements in orange). The interface is embedded between two elastic bodies (also discretized using finite elements in blue) such that the entire system is approximately square. The potential energy of blocks along the interface and in the bulk are sketched as indicated. (b) Macroscopic stress σ vs strain ε response to a quasistatic drive in which the top boundary is displaced "infinitely" slowly. After each vanishingly small step, energy is minimized by following the inertial dynamics. The position of the top boundary and the reaction force yield ε and σ (see details about units in the Appendix). "Events", during which at least one block yields, are indicated with a marker, in blue when they are system spanning.

an avalanche, a sizable fraction of the interface is slipping at any given point in time. The characteristic slip rate of an avalanche, $\dot{u}$, thus satisfies $\dot{u} \equiv S/(A^d T) \sim \dot{u}_{\min}$ that behaves as a constant as $\sigma \to \sigma^*$, which implies $T \sim A^z$ [Eq. (3)] with:

$$z = d_f - d = \zeta. \tag{11}$$

III. TESTING THE THEORY

A. A Rosetta stone model for frictional interfaces

We consider the minimal model of frictional interface containing disorder, long-range elasticity, and inertia introduced in Ref. [47]. Its details, as well as the dimensionless units we choose, are reviewed in the Appendix. As illustrated in Fig. 3(a), the frictional interface is discretized in L (orange) "blocks" of unit size. Such a mesoscopic description is standard in Burridge-Knopoff-type models [51] or in the depinning literature [26]. In the absence of inertia, it can successfully describe interfaces beyond the "Larkin length" [52], below which asperities always collectively rearrange and the details of the disorder matters. In the presence of velocity weakening, such a description can describe the interface beyond another length scale L_c, below which elastic forces dominate those stemming from velocity weakening [33–38,53]. Below we estimate L_c to be about 20 blocks in our model.

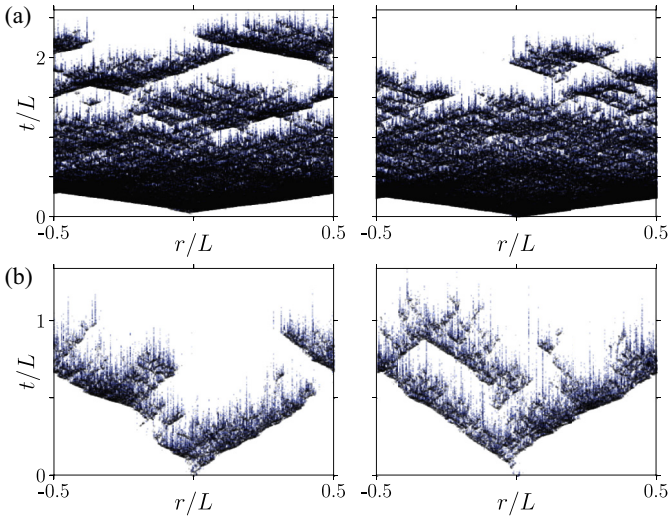

FIG. 4. Event maps for two representative system-spanning events (a) and two large avalanches nucleated at σ_c (b). A point is placed in time t and space r for each yield event (black if the block yields in the positive direction and blue if it yields in the negative direction).

The interface is embedded within two homogeneous linear elastic bodies, of total height $\approx L$, modelled by finite elements (blue).[4] The system is driven at the top and fixed at the bottom and presents periodic boundaries on the horizontal axis. Each block responds linear elastically up to a randomly chosen yield stress, whereupon it slips. This corresponds to a potential energy that, as a function of local slip, comprises a sequence of parabolic wells of random width, as illustrated in Fig. 3(a). Disorder stems from randomly choosing the yield stresses, which are proportional to the width of the wells. In the absence of inertia, such models are used to study the depinning transition [55], where they allow for fast simulations and a simple definition of avalanches, whose size S is simply the number of times blocks rearranged within an event.

We consider standard inertial dynamics, with a small damping term chosen to ensure that elastic waves become damped after propagating on a length scale of order $\sim L$, modeling the leakage of heat at the system boundary. As we show below, the presence of (weakly damped) inertia leads to a velocity weakening, well fitted by rate-and-state description. Thus, this model is ideally suited to build a dictionary between the rate-and-state description (that focuses on velocity weakening) and the depinning viewpoint (that focuses on disorder).

B. Calibrating and testing rate-and-state

1. Stationary velocity weakening

Velocity weakening is already apparent under a quasistatically imposed shear, where it leads to stick slip. As illustrated in Fig. 3(b), system-spanning events drop the stress to some value indicated in blue, are punctuated by "avalanches" in

[4]Note that in our model, frictionlike properties emerge from the presence of disorder and inertia. These properties are not prescribed form the start as in block-spring models [54].

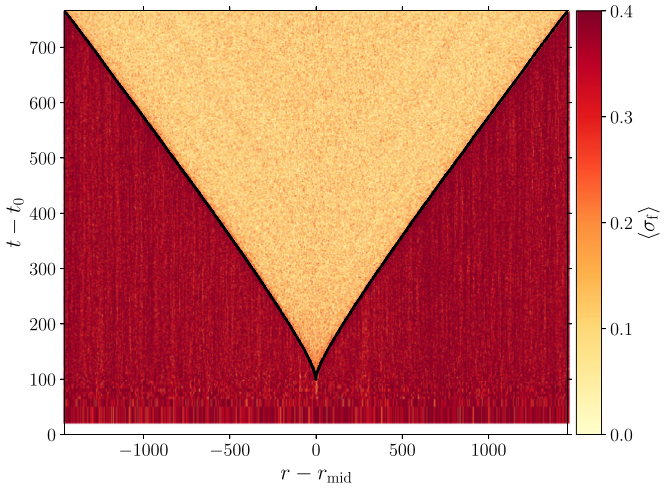

FIG. 5. Ensemble average stress $\sigma_f(r,t)$ (color) along the weak layer r (horizontal axis) as a function of time since the beginning of the event (vertical axis). The average is taken with respect to the (in general time-dependent) center of the event (details in Appendix). Identically, the average number of times a block yielded, $s(r,t)$, is recorded, whose $s(r,t) = 1$ contour is shown to delimit the front of the event.

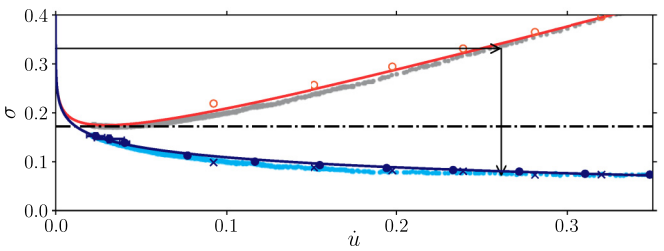

FIG. 6. In blue (solid markers): Constitutive behavior of the interfacial stress σ_f vs slip rate $\dot{u}$. The "rate-and-state" law, Eq. (12), is fitted on the solid blue markers that are measured in the steady state of a "flow experiment" in which the system is subjected to a constant shear rate. The fit is confirmed through a measurement of $(\sigma_f, \dot{u})$ during system-spanning events, as they stop ($\dot{u}$ decreases toward zero), as shown using light-blue points, truncated at low $\dot{u}$ when there are no more plastic events. In red (open markers): Effective flow curve relating the far-field stress σ to the local slip rate $\sigma = \sigma_f(\dot{u}) + \dot{u}$. The solid red curve corresponds to the fit obtained from the solid blue curve, while gray points are obtained from light-blue points. The cross-markers and open markers indicate respectively the measurements of $(\sigma_f, \dot{u})$ and $(\sigma, \dot{u})$ obtained by measuring the slip rate $\dot{u}$ and interfacial stress σ_f within a rupture occurring at an imposed stress σ. The minimum of the effective flow curve $\sigma_{\min}$ is indicated using a dash-dotted line.

which a fraction of the blocks yield (small markers). Figure 4(a) shows a spatiotemporal map of two system-spanning events spontaneously occurring on loading (i.e., at large stress), whereas Figure 4(b) illustrates two large avalanches (that we triggered directly after system spanning events, i.e., at low stress). For events nucleated at high stress, we show the average stress along the interface as a function of time in Fig. 5.[5] We use a blue contour to delimit the (average) event, using which we see that the stress drops significantly inside the event. Note that, in this work, we do not focus on the properties of the front (that travels at a velocity higher than the shear wave speed).

To describe the observed velocity weakening, we consider the rate-and-state description[6] relating the interfacial stress σ_f as a function of slip rate $\dot{u}$ and time t as $\sigma_f = \sigma_s + a\ln(\dot{u}) + b\ln[\theta(\dot{u},t)]$. Here the time dependence enters implicitly through a "state" parameter θ. Furthermore, σ_s is some offset and a and b are parameters. Usually, the state parameter is assumed to follow a simple linear ageing law $\dot{\theta} = 1 - \theta\dot{u}/D_c$. This equation captures that memory is lost once slip becomes larger than a distance D_c, beyond which the steady state ($\dot{\theta} = 0$) is reached, which implies the stationary behavior:

$$\sigma_f = \sigma_s + (a-b)\ln(\dot{u}). \tag{12}$$

Note that in frictional experiments, the "state" parameter is often associated to the real contact area. This is not the case in our model, where the contact area is fixed. Instead, we think of the state parameter as characterizing the mechanical noise stemming from inertia, that must take a finite time to reach a stationary equilibrium.

To calibrate Eq. (12), we measure the steady-state interfacial stress σ_f for different imposed slip rates $\dot{u}$, averaged in both space and time. Measurements corresponds to the solid blue markers in Fig. 6. The solid blue line fits them according to Eq. (12) and leads to $a - b \simeq -0.03$ (and $\sigma_s \simeq 0.041$).

The dynamics are intermittent at imposed $\dot{u} < \dot{u}_{\min}$ [defined in Fig. 1(b)],[7] and stick slip occurs. The response $\sigma_f(\dot{u})$ at small strain rate can be estimated by measuring evolution of the spatial average stress σ_f and the slip rate $\dot{u}$ along the weak layer in system-spanning events. After these events span the system, the average slip rate $\dot{u}$ slowly relaxes toward zero. These measurements corresponds to the light-blue points in Fig. 6 that also are well fitted by Eq. (12) with the same parameters.

As mentioned in the Introduction, in rate-and-state descriptions there is a characteristic length scale L_c beyond which velocity-weakening effects are important. As recalled in the Appendix, we can now estimate L_c using the value of $a - b$ and a natural estimate for the slip D_c where stationarity is reached. We assume that D_c corresponds to the characteristic slip length for which plasticity occurs in a given block, i.e., the typical slip for which one exits the parabolic potential in Fig. 3(a). With this, we obtain $L_c \approx 20$ blocks. In what

[5]For completeness, we average on 40 system spanning events, triggered in the highest bin of Figs. 8(e)–8(g). These results are representative of system spanning that nucleate spontaneously.

[6]We emphasize that we include only elasticity, local yielding, and inertia in our numerical model. We *do not* impose the rate-and-state model. Rather it describes the emerging properties of the interface well.

[7]Above, but close to $\dot{u}_{\min}$ intermittency still obstructs a truly steady-state measurement. We thus measure the instantaneous stress and slip rate along the interface leading to the error bars at low $\dot{u}$.

follows, we focus on the quantification of slip events that are larger than L_c.

2. *Radiation damping leads to a nonmonotonic effective flow curve*

The blue curve in Fig. 6 describes a stationary situation. However, when a slip event occurs and has not yet spanned the entire system, it must accelerate the elastic material around it. This phenomenon must obviously occur here as well, since we realistically describe the elastic material around the interface. Zheng and Rice [8] show that it is captured by a "radiation damping" term, describing the difference between the stress in the far field σ and that of the interface σ_f during an event that is growing in space. In our dimensionless units (see the Appendix), it simply reads:

$$\sigma = \sigma_f(\dot{u}) + \dot{u}. \tag{13}$$

We show the far-field stress σ in red in Fig. 6. A key observation is that this curve is nonmonotonic and presents a minimum $\sigma_{\min} \approx 0.17$. Following previous works [8,40], nucleation of a system-spanning, cracklike, event in homogeneous systems is possible beyond some stress $\sigma^* \approx \sigma_{\min}$. Below we will support empirically our prediction that σ^* is also the stress σ_c where avalanches display a diverging cut-off.

Another prediction of rate-and-state (less relevant to our present purpose but useful to further support the predictive power of rate-and-state in our model) is that when a system-spanning event starts to invade the material, away from the rupture front the local stress and slip rate can be readily extracted from Eq. (13), see Barras *et al.* [56]. This result is illustrated using the arrows in Fig. 6, showing that for a given imposed stress σ (horizontal arrow), $\dot{u}$ and σ_f within system-spanning events can be read from this curve (vertical arrow). We confirm this construction in Fig. 6: The open markers indicate the applied stress σ and the observed slip rate $\dot{u}$. The cross-markers instead indicate the interfacial stress σ_f inside the event and $\dot{u}$. We indeed find that $(\sigma_f, \dot{u})$ away from the rupture front closely follow the identified steady-state flow curve.

C. Statistics of slip events

We now test the (i) scaling relations we derived earlier for slip events and (ii) the correspondence between the stress σ_c where avalanches diverge and the rate-and-state characteristic stress $\sigma_{\min}$, in the neighborhood of which nucleation of unstable rupture front is predicted in homogeneous systems, at $\sigma^* \gtrsim \sigma_{\min}$ [40].

1. *Interface roughness*

As discussed in the theoretical section, the fluctuation of the strength of the interface $\delta\sigma^*$ must be reflected in the fluctuations $\delta\sigma_f$ of the physical stress carried by the interface, since slip will tend to occur until the mean stress in a region of size A, $\sigma_f(A)$, has relaxed toward $\sigma^*(A)$. We have no direct measurement of $\sigma^*(A)$. Instead, we study $\sigma_f(A)$ and its fluctuation $\delta\sigma_f(A)$. We consider the system directly after 4000 system-spanning events,[8] indicated in blue in Fig. 3(b). We randomly choose patches of linear length A along the interface and compute the average stress in each patch. We then measure the mean and the standard deviation $\delta\sigma_f(A)$ for different length A. In Fig. 7(a), we confirm the power-law behavior $\delta\sigma_f(A) \sim A^{-\chi}$, from which we gain an estimate of the exponent χ entering Eq. (6) [assuming $\delta\sigma_f(A) \approx \delta\sigma^*(A)$].

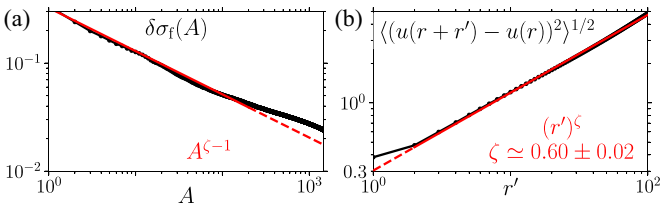

FIG. 7. (a) Standard deviation of the distribution of mean interfacial stress σ_f on a patch of blocks of size A as a function of A. In particular, we measure std($\{\sum_{i=j}^{j+A} \sigma_i/A\}$) (with i the index of a block along the weak layer), with the set $\{\ldots\}$ coming from choosing j at random locations in each realization of the ensemble; see the Appendix for a precise statement. (b) Roughness exponent ζ measured from the mean-square fluctuations of slip (note that a spatial average on r is implied). The error bar on ζ includes both statistical errors (estimated from a least-squares regression) and systematic biases (estimated by reducing the fitting range), as detailed in the Appendix.

Such stress fluctuations must affect the roughness of the interface, as argued above. We confirm this view in Fig. 7(b), which displays the relationship between the slip fluctuations $||u(r) - u(r')||$ and the distance $||r - r'||$. This observation confirms a power law postulated in Eq. (5) with an exponent $\zeta \simeq 0.60$, a measurement consistent with the scaling relation $\chi = 1 - \zeta$ of Eq. (7).

2. *Statistics of avalanches*

To acquire a large statistics, we follow the strategy in Ref. [47] of manually triggering 9000 events such as in Fig. 4(b), using a local perturbation at imposed strain, following a system spanning event. The postmortem effect of such an avalanche on the slip profile is shown in Fig. 8(a), illustrating the definitions of the spatial extension A and the total slip S. As shown in Figs. 8(b)–8(d), we confirm power-law behaviors for the distribution of avalanches $P(S) \sim S^{-\tau}$, the avalanche geometry $S \sim A^{d_f}$, and duration $T \sim A^z$; with $\tau \approx 1.77$, $z \approx 0.64$[9] and $d_f \approx 1.60$.

[8] Which is about 10% of the total number of events that occur during quasistatic loading.

[9] An exponent $z < 1$ is asymptotically impossible, since it would lead to a diverging propagation speed $v \sim A^{1-z}$ for large events. Once the speed of sound is reached, one presumably finds $z = 1$. At that point, our hypothesis on the existence of a characteristic slip rate of avalanches must break down, instead we expect this rate to decrease with A. However, this limit is presumably very hard to reach empirically. In our system, we estimate that the speed of sound would be reached for $A = 40\,000$ blocks or $2000L_c$, far beyond what we can achieve numerically. This crossover is also presumably not observable in earthquakes, since L_c is believed to be kilometric in faults.

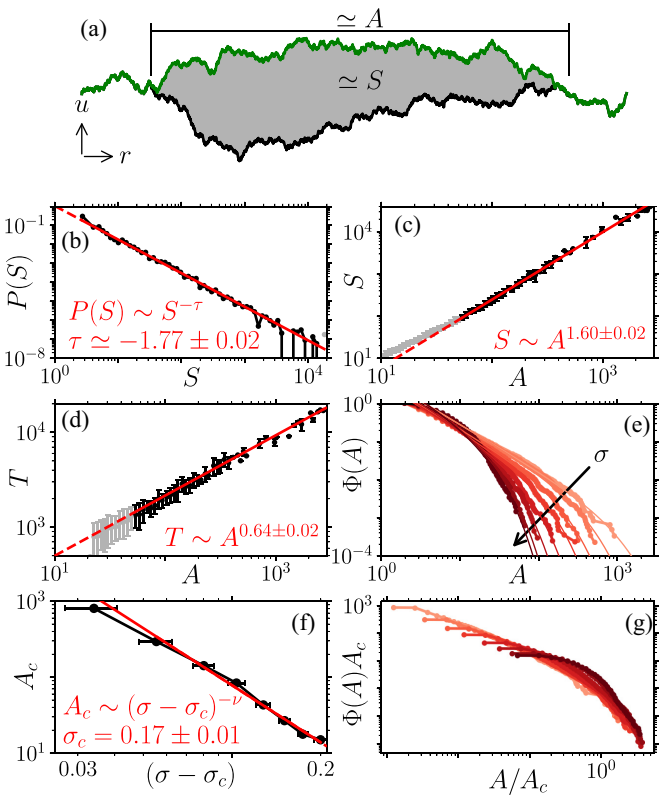

FIG. 8. [(a)–(d)] Example of slip profile $u(r)$ before (bottom black curve) and after (top green curve) an avalanche. The linear extension A and total slip S are schematically indicated. Our results are consistent with $P(S) \sim S^{-\tau}$ (b), $S \sim A^{1+\zeta}$ (c), and avalanche duration $T \sim A^{\zeta}$ (d). (e) Cumulative probability $\Phi(A)$ of avalanches (whose $A < L$) triggered at different stresses σ. The thin line indicates a fit $\Phi(A) \sim A^{1-\tau_A} \exp(-A/A_c)$. Indeed, the obtained $A_c(\sigma)$ collapses our data (g). (f) Fit of the offset σ_c such that $A_c \sim (\sigma - \sigma_c)^{-\nu}$, while imposing our prediction for ν in Eq. (9).

3. Nucleation size

To estimate the nucleation size A_c beyond which an avalanche becomes a rupture front spanning the system, we measure the cumulative distribution of avalanche elongation $\Phi(A)$ at various stress levels, as shown in Fig. 8(e). Next we fit $\Phi(A) \sim A^{1-\tau_A} \exp(-A/A_c)$ [10] so as to extract A_c. In Fig. 8(f), we confirm that rescaling $\Phi(A)$ by such an obtained A_c indeed collapses the different curves. There is a considerable empirical indeterminacy on the exponent ν entering $A_c \sim (\sigma - \sigma_c)^{-\nu}$, because the value of σ_c is not known *a priori*. To proceed, we impose the predicted value $\nu = 1/(1-\zeta)$ with $\zeta = 0.60$ and choose σ_c to obtain the best power-law behavior, as displayed in Fig. 8(f). We obtain a good fit, showing that ν is consistent with our prediction. Most importantly, we get $\sigma_c \approx 0.17 \pm 0.01$ which is consistent with the value $\sigma_{\min} \approx 0.17$ extracted from the effective flow curve. Since rate-and-state predicts a threshold for unstable slip events at $\sigma^* \approx \sigma_{\min}$, our observations support that σ^* indeed controls avalanches in disordered frictional interfaces.

[10] $\tau_A = 1 + (\tau - 1)(1 + \zeta)$ as follows from Eqs. (1), (2), and (10).

TABLE I. Overview of results: scaling predictions and measured exponents in our $d = 1$ system. We report the fitted exponents in Figs. 7 and 8. The uncertainty sums the statistical error plus an estimate of the systematic error stemming from the finite system size (which is estimated by considering the change in exponent in a twice smaller system).

Scaling	Prediction	Measurement
$P(S) \sim S^{-\tau}$	—	1.77 ± 0.25
$\delta u(r) \sim r^{\zeta}$	—	0.60 ± 0.08
$S \sim A^{d_f}$	$1 + \zeta \simeq 1.60$	1.60 ± 0.09
$T \sim A^{z}$	$\zeta \simeq 0.60$	0.64 ± 0.06
$A_c \sim (\delta\sigma)^{-\nu}$	$1/(1-\zeta) \simeq 2.5$	2.25 ± 0.77

4. Summary of results

The set of exponents measured are reported in Table I. d_f and z are in excellent agreement with our predictions (ν is nicely consistent with those but cannot be extracted precisely).

These exponents differ markedly from those obtained in the absence of inertia with the same dimension $d = 1$ and long-range interactions, for which it is found numerically that $\zeta \in [0.34, 0.39]$ [57–62]. These values are in reasonable agreement with renormalization group (RG) predictions [60,63,64]. However, RG has not been successfully developed when velocity weakening is important. In that case, our results indicate the existence of a new universality class.

At the experimental level, crack propagation [65–67] and contact line experiments [68,69] often report $\zeta \in [0.5, 0.7]$. These exponents are closer to our predictions, yet it is unclear if inertia is responsible for this discrepancy with over-damped numerical observations [57–62], or if other effects are at play [67].

IV. CONCLUSION AND PERSPECTIVE

A. Summary

We have introduced a theoretical framework for the nucleation and statistics of slip at a disordered frictional interface. It builds on rate-and-state results [8,40] showing that in the presence of strong velocity-weakening effects, a homogeneous system presents a threshold stress σ^* beyond which a rupture can invade the system. We have argued that in the presence of disorder, such a threshold must lead to power-law avalanches. Rupture occurs when one avalanche becomes larger than some size A_c beyond which the disorder becomes negligible and cannot stop a rupture. A_c diverges as $\sigma \to \sigma^*_+$ with some new exponent. This framework leads to quantitative predictions, partly based on extending arguments from the depinning literature [42], where the threshold stress can be defined statically, to situations where the threshold is dynamically defined. Most importantly, our theoretical approach should stand as long as the frictional interface is well described by rate-and-state, irrespectively of the underlying mechanism causing velocity weakening. Note that we have numerically checked this prediction only in a specific model, leaving a check to broader classes of models for future work.

Next we used a minimal model of frictional interface as a Rosetta stone, in which (i) rate-and-state equations can

be calibrated and their predictions tested and (ii) disorder is easily controllable and slip statistics readily measurable. It allowed for a stringent test of our scaling predictions and put forward numerical values for exponents that future theories should seek to explain.

B. Geophysical data

We have argued that for a disordered but overall flat velocity-weakening frictional interface, the distribution of slip events should be bimodal. Power-law-distributed avalanches are present, which display scaling properties. We find, for example, a scaling relationship between the avalanche size or "seismic moment"[11] S and its associated stress drop $\delta\sigma_f \sim S^{-1/(d_f \nu)} \sim S^{-0.25}$. In the geophysics literature, these empirical facts are debated. Some studies report that the stress drop mildly decreases [70] or increases [71] with the earthquake size. Furthermore, as noted in the Introduction, for a single fault bimodal [17] or monomodal [18] slip distributions have been argued for. In our opinion, the interpretation of these results is complicated by the geometry of faults, which display broadly distributed segments where slip can occur [19]. We view our theoretical results as a first step focusing on a simple interface geometry. Arguably, more complex geometrical factor must be included to rationalize geophysical observations. In this respect, it would be very interesting to consider a frictional interface made of power-law-distributed segments. It can be readily implemented in our model, where the geometry of plastic regions where slip occurs can be chosen at will.

C. Future works

More generally, our methodology corresponds to a minimal model with a desired rate-and-state behavior. In the future, controlled disorder can be used to incorporate other phenomena of interest and study how they shape slip statistics. A particularly relevant case is thermal creep, which is expected to lead to an N-shaped effective flow curve, which can be readily obtained by simulating the dynamics in our model at finite temperature. Likewise, the materials surrounding the interface can be viscoelastic instead of elastic, which is a sufficient condition (but not always necessary [72]) to obtain aftershocks [73].

ACKNOWLEDGMENTS

We thank A. Rosso, J.-F. Molinari, T.D. Roch, M.A.D. Lebihain, M. Popović, E. Agoritsas, W. Ji, M. Violay, and M. Müller for discussions and J. Volmer and F. Barras for feedback on the manuscript. T.G. acknowledges support from the Swiss National Science Foundation (SNSF) by the SNSF Ambizione Grant No. PZ00P2_185843. M.W acknowledges support from the Simons Foundation Grant No. 454953 Matthieu Wyart and from the SNSF under Grant No. 200021-165509.

APPENDIX: DETAILS OF THE MODEL

1. Equation of motion

We consider standard continuum elastodynamics, so that the equation of motion reads

$$\tilde{\rho}\partial_{\tilde{t}}^2 \tilde{w}_i(r) = \mathrm{div}[\tilde{\sigma}_{ij}(r)] - \tilde{\alpha}\partial_{\tilde{t}}\tilde{w}_i(r), \tag{A1}$$

where $\tilde{w}_i(r)$ is the displacement field (a function of position r, whose vectorial nature is omitted for notational simplicity) and $\partial_{\tilde{t}}\tilde{w}_i$ and $\partial_{\tilde{t}}^2\tilde{w}_i$ its first and second time derivative. $\tilde{\rho}$ is the mass density and $\tilde{\alpha}$ is the (small) damping coefficient, both are taken homogeneous. $\mathrm{div}[\tilde{\sigma}_{ij}(r)]$ is the divergence of the stress tensor $\tilde{\sigma}_{ij}$. The latter follows from linear elasticity, which we model as

$$\tilde{\sigma}_{ij}(r) = [\tilde{\kappa}/(d+1)]\mathrm{tr}[\tilde{\varepsilon}_{ij}(r)]\delta_{ij} + 2\tilde{\mu}[\tilde{u}(r) - \tilde{u}_{\min}(r)]N_{ij}(r). \tag{A2}$$

Here $\tilde{\varepsilon}_{ij}(r) = [\partial_i\tilde{w}_j(r) + \partial_j\tilde{w}_i(r)]/2$ is the strain tensor. $d+1$ [12] is the dimension of the bodies (here $d+1=2$), $\tilde{\kappa}$ is the bulk modulus, $\tilde{\mu}$ is the shear modulus, δ_{ij} is the unit tensor, and $\mathrm{tr}(a_{ij}) = a_{ij}\delta_{ij}$ is the trace of a_{ij}. $N_{ij}(r)$ defines the direction of shear as

$$N_{ij}(r) = \mathrm{dev}[\tilde{\varepsilon}_{ij}(r)]/\tilde{u}(r), \tag{A3}$$

where $\mathrm{dev}[\tilde{\varepsilon}_{ij}(r)]$ is the deviatoric (trace-free) part of the strain tensor and

$$\tilde{u}(r) \equiv ||\tilde{\varepsilon}_{ij}(r)||_d \equiv (\mathrm{dev}[\tilde{\varepsilon}_{ij}(r)]\mathrm{dev}[\tilde{\varepsilon}_{ij}(r)]/2)^{1/2} \tag{A4}$$

corresponds to the magnitude of the shear strain, which we refer to as "slip". Likewise, we define the magnitude of shear stress

$$||\tilde{\sigma}_{ij}(r)||_d \equiv (2\,\mathrm{dev}[\tilde{\sigma}_{ij}(r)]\mathrm{dev}[\tilde{\sigma}_{ij}(r)])^{1/2}. \tag{A5}$$

The potential energy landscape in Fig. 3(a) is defined along $\tilde{u}(r)$, with $\tilde{u}_{\min}(r)$ the currently closest local minimum along the coordinate $\tilde{u}(r)$. It is always equal to zero in the bulk [in blue in Fig. 3(a)], but typically finite along the "weak" layer [in red in Fig. 3(a)]. Along that layer, the cusps are separated by a distance chosen randomly from a Weibull distribution that has a typical value $2\tilde{u}_0$.

2. Units

A typical magnitude of shear strain is the typical yield strain $\tilde{u}_0$ of a block, which we use to define units, such that $\varepsilon_{ij}(r) \equiv \tilde{\varepsilon}_{ij}(r)/\tilde{u}_0$ and $\sigma_{ij}(r) \equiv \tilde{\sigma}_{ij}(r)/\tilde{\sigma}_0$ with $\tilde{\sigma}_0 \equiv 4\tilde{\mu}\tilde{u}_0$. Thereby, we denote dimensionless quantities $\bullet$ and their dimension-full equivalent $\tilde{\bullet}$.

We define the plastic slip $u_p(r) \equiv \tilde{u}_{\min}(r)/\tilde{u}_0$ as the location of the current local minimum in dimensionless slip space, see Fig. 3(a). These definitions are such that, on average, the

[11] The seismic moment is defined as the average slip times the slipping area, times the shear modulus. Our definition of S is a proxy for the former product, taking that the slip of a block is proportional to the number of times the block yields, and assuming that A is a proxy for the linear extension of the avalanche which we justify by the observation that avalanches a compact—each block yields many times during an avalanche, see Fig. 4.

[12] We use d as the dimension of the interface.

number of times a block yields $s(r) = \Delta u_p(r)/2 \approx \Delta u(r)/2$. The slip rate $\dot{u} \equiv \Delta u/\Delta t$, with time $t \equiv \tilde{t}/\tilde{t}_0$, where $\tilde{t}_0 \equiv \tilde{\ell}_0/\tilde{c}_s$ with $\tilde{c}_s$ the shear wave speed. We note that length is expressed in units of $\tilde{\ell}_0$ such that $L \equiv \tilde{L}/\tilde{\ell}_0$ and $\ell_0 \equiv \tilde{\ell}_0/\tilde{\ell}_0 = 1$. In our dimensionless units, slip at the interface, that we define as the strain in the blocks, thus coincides with the displacement discontinuity across the interface. Furthermore, time t indicates the number of blocks a shear wave traversed. A slip rate $\dot{u}(r) = 0.5$ thus indicates that a typical block yields once during time it takes a shear wave to travel the distance of one block.

We extract the total slip $S \equiv \int_L s(r)dr$ ($\int_L \dots dr$ denotes the integral along the weak layer) as the total number of times blocks yield, A the number of blocks that yield at least once (thus $A \equiv \int_L [s(r) + |s(r)|]/[2|s(r)|]dr$), and T the (dimensionless) duration between the first and the last time that a block yield during an event.

3. Numerical model

The numerical treatment of this equation of motion corresponds to a discretization in space using finite elements [where at the weak layer the elements coincide with the blocks of linear size $\tilde{\ell}_0$, see Fig. 3(a)] and in time using the velocity Verlet algorithm. The numerical values of all parameters, and more details, can be found in Refs. [47,74]. Different from those references, here we consider a bigger system of $L = 4 \times 3^6$ blocks (except for the results in Fig. 4 which are made on the system of Ref. [47]), and a 10-times-smaller typical strain $\tilde{u}_0$ to acquire more events per realization while respecting the small strain assumption. Note that this does not lead to any change in terms of the dimensionless quantities reported here and in Ref. [47]. In addition, we perform flow experiments by imposing a fixed shear rate to the top boundary. In practice, the shear is supplied to the system in a distributed manner, such that in each time step all nodal displacements are updated according to an affine simple shear, though only the top boundary is fixed. We measure both σ_f and $\dot{u}$ as averaged in space along the interface and on a finite window of time deep in the steady state, as well as on different realizations.

4. Quantities

The remote stress is the volume averaged shear stress,

$$\sigma \equiv \left\| \iint_L \boldsymbol{\sigma}(\vec{r})\, d\vec{r} \right\|_d = \sum_{\beta=1}^{n} (\tilde{f}_x)_\beta / (n\tilde{\ell}_0\tilde{\sigma}_0), \tag{A6}$$

with $\boldsymbol{\sigma}(\vec{r})$ the adimensional stress tensor at a position $\vec{r}$ in $(d+1)$-dimensional space and $\iint_L \dots dr$ the integral over the entire domain in $(d+1)$-dimensional space. $(\tilde{f}_x)_\beta$ are the reaction forces in horizontal direction of the $n+1$ nodes along the top boundary (one node is "virtual" because of the periodic boundary conditions in horizontal direction) whose position is prescribed. The remote strain is the volume averaged strain,

$$\varepsilon \equiv \left\| \iint_L \boldsymbol{\varepsilon}(\vec{r})\, d\vec{r} \right\|_d = (\tilde{w}_x)_\beta / (\tilde{H}\tilde{u}_0), \tag{A7}$$

with $(\tilde{w}_x)_\beta$ the displacement in horizontal direction of one of the nodes along the top boundary (the displacement of all of these nodes is definition equal), and $\tilde{H} \approx L\tilde{\ell}_0$ the actual height of the sample.

The stress along the interface

$$\sigma_f \equiv \left\| \int_L \boldsymbol{\sigma}(r)\, dr \right\|_d = \left\| \sum_{i=1}^{L} \boldsymbol{\sigma}_i \right\|_d, \tag{A8}$$

with i referring the block index along the weak layer (numbered from left to right). We note that

$$\sigma_f(A) = \left\| \sum_{i=j}^{i+A} \boldsymbol{\sigma}_i \right\|_d \tag{A9}$$

(where periodicity implies $\boldsymbol{\sigma}_i = \boldsymbol{\sigma}_{i+L}$).

The slip along the interface is

$$u \equiv \left\| \int_L \boldsymbol{\varepsilon}(r)\, dr \right\|_d = \left\| \sum_{i=1}^{L} \boldsymbol{\varepsilon}_i \right\|_d. \tag{A10}$$

Finally, the slip rate is

$$\dot{u} \equiv \left\| \int_L \partial_t \boldsymbol{\varepsilon}(r)\, dr \right\|_d = \left\| \sum_{i=1}^{L} \partial_t \boldsymbol{\varepsilon}_i \right\|_d. \tag{A11}$$

5. Radiation damping

A nucleating event, whereby part of the interface and bulk are still static as the rupture invades the interface, is stabilized by the bulk surrounding it: To increase the slip rate $\dot{u}$ the bulk around the rupture has to be accelerated. Due to the cost of accelerating an expanding volume, the interfacial stress σ_f inside the event differs from the remote stress σ. Because the bulk is accelerated by elastic waves that radiate away from the interface this effect is commonly referred to as "radiation damping". We emphasize that this is an effect of standard elastodynamics: It is not added by hand to our model.

The effect of radiation damping corresponds to a "cost" of stress [8] $\Delta\tilde{\sigma}_{xy} = \tilde{v}\tilde{\mu}/(2\tilde{c}_s)$, with $\tilde{v} \equiv 2\Delta(\delta\tilde{r}_x)/\Delta\tilde{t}$ [75] the rate of change of the displacement discontinuity $\delta\tilde{r}_x \equiv 2\tilde{\varepsilon}_{xy}\tilde{\ell}_0 = 2\tilde{u}\tilde{\ell}_0$ such that $\Delta\tilde{\sigma} = (4\Delta\tilde{u}\tilde{\ell}_0/\Delta\tilde{t})(\tilde{\mu}/\tilde{c}_s) = 4\tilde{\mu}\Delta\tilde{u}/(\Delta\tilde{t}/\tilde{t}_0)$ or $\Delta\tilde{\sigma}/(4\tilde{\mu}\tilde{u}_0) = (\Delta\tilde{u}/\tilde{u}_0)/(\Delta\tilde{t}/\tilde{t}_0)$ and thus $\Delta\sigma = \dot{u}$.

6. Computation of L_c

For the rate-and-state law $\tilde{L}_c = -\pi\tilde{\mu}\tilde{D}_c/(\dot{\tilde{u}}\partial\tilde{\sigma}/\partial\dot{\tilde{u}})$ [40] with $\partial\tilde{\sigma}/\partial\dot{\tilde{u}} = (\tilde{a} - \tilde{b})/\dot{\tilde{u}}$ the derivative of the steady state in Eq. (12), such that $\tilde{L}_c = -\pi\tilde{\mu}\tilde{D}_c/(\tilde{a} - \tilde{b})$. In our model, a block, on average, loses memory over a sliding distance $\tilde{D}_c = \tilde{u}_0\tilde{\ell}_0$. Using, furthermore, our units of stress such that $a = \tilde{a}/\tilde{\sigma}_0$ and $b = \tilde{b}/\tilde{\sigma}_0$, we find $\tilde{L}_c = -\pi\tilde{\mu}\tilde{u}_0\tilde{\ell}_0/[\tilde{\sigma}_0(a - b)] = -\pi\tilde{\ell}_0/[4(a - b)]$, and thus $L_c = -\pi/[4(a - b)] \approx 26$.

7. Power-law fits

The power-law fit of $y = cx^b$ is performed using a least-squares fit of the linear relation $z \equiv \ln y = \ln c + b \ln x$. In the case of an uncertainty δy (typically a standard deviation) we assume that $\delta y \ll y$ such that we use $\delta z = \delta y/y$. The error of the fitted exponent, δb_f, is then the square root of the relevant component at the diagonal of the 2×2 covariance matrix.

Where possible, we also compute the fluctuations of the exponent, δb_ℓ, by reducing the fitting range by factors of two and four. We report δb_ℓ in Fig. 7(b), and δb_f in Figs. 8(b)–8(d) [in Figs. 8(b) and 8(c) the δb_ℓ was simply found lower or equal to δb_ℓ; in Fig. 8(d) the range is not sufficient to be reduced].

In Fig. 8(f) we account for the error in σ by taking the error as dimensionless, allowing us to compose it in equal amounts of the errors in σ (the standard deviation of σ in each bin) and in A_c [the fitting error from Fig. 8(e)]. We use this protocol also to fit ν given $\sigma_{\min} \approx 0.17$ as reported in Table I.

In Table I we estimate the error on ν as the difference between our prediction and a fit of the exponent of the data in Fig. 8(f) using σ_c defined as the bottom of the effective flow curve in Fig. 6.

[1] J. R. Rice, Spatio-temporal complexity of slip on a fault, J. Geophys. Res. **98**, 9885 (1993).

[2] C. H. Scholz, Earthquakes and friction laws, Nature (London) **391**, 37 (1998).

[3] K. Xia, A. J. Rosakis, and H. Kanamori, Laboratory earthquakes: The sub-Rayleigh-to-supershear rupture transition, Science **303**, 1859 (2004).

[4] S. M. Rubinstein, G. Cohen, and J. Fineberg, Detachment fronts and the onset of dynamic friction, Nature (London) **430**, 1005 (2004).

[5] O. Ben-David, S. M. Rubinstein, and J. Fineberg, Slip-stick and the evolution of frictional strength, Nature (London) **463**, 76 (2010).

[6] F. X. Passelègue, A. Schubnel, S. B. Nielsen, H. S. Bhat, and R. Madariaga, From sub-Rayleigh to supershear ruptures during stick-slip experiments on crustal rocks, Science **340**, 1208 (2013).

[7] T. H. Heaton, Evidence for and implications of self-healing pulses of slip in earthquake rupture, Phys. Earth Planet. Inter. **64**, 1 (1990).

[8] G. Zheng and J. R. Rice, Conditions under which velocity-weakening friction allows a self-healing versus a cracklike mode of rupture, Bull. Seismol. Soc. Am. **88**, 1466 (1998).

[9] T. Roch, E. A. Brener, J.-F. Molinari, and E. Bouchbinder, Velocity-driven frictional sliding: Coarsening and steady-state pulses, J. Mech. Phys. Solids **158**, 104607 (2022).

[10] I. Svetlizky and J. Fineberg, Classical shear cracks drive the onset of dry frictional motion, Nature (London) **509**, 205 (2014).

[11] I. Svetlizky, D. Pino Muñoz, M. Radiguet, D. S. Kammer, J.-F. Molinari, and J. Fineberg, Properties of the shear stress peak radiated ahead of rapidly accelerating rupture fronts that mediate frictional slip, Proc. Natl. Acad. Sci. USA **113**, 542 (2016).

[12] O. Ben-David and J. Fineberg, Static Friction Coefficient is Not a Material Constant, Phys. Rev. Lett. **106**, 254301 (2011).

[13] V. L. Popov, *Contact Mechanics and Friction* (Springer, Berlin, 2010).

[14] E. Rabinowicz, Friction coefficients of noble metals over a range of loads, Wear **159**, 89 (1992).

[15] W. F. Brace and J. D. Byerlee, Stick-s as a mechanism for earthquakes, Science **153**, 990 (1966).

[16] B. U. Gutenberg and C. F. Richter, *Seismicity of the Earth and Related Phenomena* (Princeton University Press, Princeton, NJ, 1954).

[17] S. G. Wesnousky, The Gutenberg-Richter or characteristic earthquake distribution, which is it? Bull. Seismol. Soc. Am. **84**, 1940 (1994).

[18] M. T. Page, D. Alderson, and J. Doyle, The magnitude distribution of earthquakes near Southern California faults, J. Geophys. Res. **116**, B12309 (2011).

[19] I. Manighetti, D. Zigone, M. Campillo, and F. Cotton, Self-similarity of the largest-scale segmentation of the faults: Implications for earthquake behavior, Earth Planet. Sci. Lett. **288**, 370 (2009).

[20] C. H. Scholz and J. T. Engelder, The role of asperity indentation and ploughing in rock friction—I, Int. J. Rock Mech. Min. Sci. Geomech. Abstr. **13**, 149 (1976).

[21] T. Baumberger and C. Caroli, Solid friction from stick–slip down to pinning and aging, Adv. Phys. **55**, 279 (2006).

[22] E. Rabinowicz, Stick and slip, Sci. Am. **194**, 109 (1956).

[23] C. Marone, Laboratory-derived friction laws and their application to seismic faulting, Annu. Rev. Earth Planet. Sci. **26**, 643 (1998).

[24] F. Heslot, T. Baumberger, B. Perrin, B. Caroli, and C. Caroli, Creep, stick-slip, and dry-friction dynamics: Experiments and a heuristic model, Phys. Rev. E **49**, 4973 (1994).

[25] T. Vincent-Dospital, R. Toussaint, S. Santucci, L. Vanel, D. Bonamy, L. Hattali, A. Cochard, E. G. Flekkøy, and K. J. Måløy, How heat controls fracture: The thermodynamics of creeping and avalanching cracks, Soft Matter **16**, 9590 (2020).

[26] D. S. Fisher, K. A. Dahmen, S. Ramanathan, and Y. Ben-Zion, Statistics of earthquakes in simple models of heterogeneous faults, Phys. Rev. Lett. **78**, 4885 (1997).

[27] S. Ramanathan, D. Ertaş, and D. S. Fisher, Quasistatic Crack Propagation in Heterogeneous Media, Phys. Rev. Lett. **79**, 873 (1997).

[28] J. M. Schwarz and D. S. Fisher, Depinning with Dynamic Stress Overshoots: Mean Field Theory, Phys. Rev. Lett. **87**, 096107 (2001).

[29] K. M. Salerno, C. E. Maloney, and M. O. Robbins, Avalanches in Strained Amorphous Solids: Does Inertia Destroy Critical Behavior?, Phys. Rev. Lett. **109**, 105703 (2012).

[30] J. H. Dieterich, Modeling of rock friction: 1. Experimental results and constitutive equations, J. Geophys. Res. **84**, 2161 (1979).

[31] J. R. Rice and A. L. Ruina, Stability of steady frictional slipping, J. Appl. Mech. **50**, 343 (1983).

[32] A. L. Ruina, Slip instability and state variable friction laws, J. Geophys. Res. **88**, 10359 (1983).

[33] M. Lebihain, T. Roch, M. Violay, and J.-F. Molinari, Earthquake nucleation along faults with heterogeneous weakening rate, Geophys. Res. Lett. **48**, 21 (2021).

[34] H. Perfettini, M. Campillo, and I. Ionescu, On the scaling of the slip weakening rate of heterogeneous faults, J. Geophys. Res. **108**, (2003).

[35] S. Ray and R. C. Viesca, Earthquake nucleation on faults with heterogeneous frictional properties, normal stress, J. Geophys. Res. Solid Earth **122**, 8214 (2017).

[36] P. Dublanchet, The dynamics of earthquake precursors controlled by effective friction, Geophys. J. Int. **212**, 853 (2018).

[37] G. Albertini, S. Karrer, M. D. Grigoriu, and D. S. Kammer, Stochastic properties of static friction, J. Mech. Phys. Solids **147**, 104242 (2021).

[38] S. Schär, G. Albertini, and D. S. Kammer, Nucleation of frictional sliding by coalescence of microslip, Int. J. Solids Struct. **225**, 111059 (2021).

[39] M. Ohnaka and Y. Kuwahara, Characteristic features of local breakdown near a crack-tip in the transition zone from nucleation to unstable rupture during stick-slip shear failure, Tectonophysics **175**, 197 (1990).

[40] E. A. Brener, M. Aldam, F. Barras, J. F. Molinari, and E. Bouchbinder, Unstable Slip Pulses and Earthquake Nucleation as a Nonequilibrium First-Order Phase Transition, Phys. Rev. Lett. **121**, 234302 (2018).

[41] D. S. Fisher, Threshold Behavior of Charge-Density Waves Pinned by Impurities, Phys. Rev. Lett. **50**, 1486 (1983).

[42] D. S. Fisher, Collective transport in random media: From superconductors to earthquakes, Phys. Rep. **301**, 113 (1998).

[43] K. A. Dahmen, D. Ertaş, and Y. Ben-Zion, Gutenberg-Richter and characteristic earthquake behavior in simple mean-field models of heterogeneous faults, Phys. Rev. E **58**, 1494 (1998).

[44] J. M. Schwarz and D. S. Fisher, Depinning with dynamic stress overshoots: A hybrid of critical and pseudohysteretic behavior, Phys. Rev. E **67**, 021603 (2003).

[45] R. Maimon and J. M. Schwarz, Continuous Depinning Transition with an Unusual Hysteresis Effect, Phys. Rev. Lett. **92**, 255502 (2004).

[46] A. Baldassarri, F. Dalton, A. Petri, S. Zapperi, G. Pontuale, and L. Pietronero, Brownian Forces in Sheared Granular Matter, Phys. Rev. Lett. **96**, 118002 (2006).

[47] T. W. J. de Geus, M. Popović, W. Ji, A. Rosso, and M. Wyart, How collective asperity detachments nucleate slip at frictional interfaces, Proc. Natl. Acad. Sci. USA **116**, 23977 (2019).

[48] B. Gutenberg and C. F. Richter, Frequency of earthquakes in California, Bull. Seismol. Soc. Am. **34**, 185 (1944).

[49] Y. Y. Kagan, *Earthquakes: Models, Statistics, Testable Forecasts* (John Wiley & Sons Inc., New York, 2014).

[50] J. T. Chayes, L. Chayes, D. S. Fisher, and T. Spencer, Finite-Size Scaling and Correlation Lengths for Disordered Systems, Phys. Rev. Lett. **57**, 2999 (1986).

[51] R. Burridge and L. Knopoff, Model and theoretical seismicity, Bull. Seismol. Soc. Am. **57**, 341 (1967).

[52] X. Cao, S. Bouzat, A. B. Kolton, and A. Rosso, Localization of soft modes at the depinning transition, Phys. Rev. E **97**, 022118 (2018).

[53] K. Uenishi and J. R. Rice, Universal nucleation length for slip-weakening rupture instability under nonuniform fault loading, J. Geophys. Res. **108**, (2003).

[54] J. S. Langer, J. M. Carlson, C. R. Myers, and B. E. Shaw, Slip complexity in dynamic models of earthquake faults, Proc. Natl. Acad. Sci. USA **93**, 3825 (1996).

[55] E. A. Jagla, Different universality classes at the yielding transition of amorphous systems, Phys. Rev. E **96**, 023006 (2017).

[56] F. Barras, M. Aldam, T. Roch, E. A. Brener, E. Bouchbinder, and J.-F. Molinari, Emergence of Cracklike Behavior of Frictional Rupture: The Origin of Stress Drops, Phys. Rev. X **9**, 041043 (2019).

[57] S. Ramanathan and D. S. Fisher, Onset of propagation of planar cracks in heterogeneous media, Phys. Rev. B **58**, 6026 (1998).

[58] A. Rosso and W. Krauth, Roughness at the depinning threshold for a long-range elastic string, Phys. Rev. E **65**, 025101(R) (2002).

[59] A. A. Middleton, Asymptotic Uniqueness of the Sliding State for Charge-Density Waves, Phys. Rev. Lett. **68**, 670 (1992).

[60] O. Narayan and D. S. Fisher, Threshold critical dynamics of driven interfaces in random media, Phys. Rev. B **48**, 7030 (1993).

[61] A. Tanguy, M. Gounelle, and S. Roux, From individual to collective pinning: Effect of long-range elastic interactions, Phys. Rev. E **58**, 1577 (1998).

[62] O. Duemmer and W. Krauth, Depinning exponents of the driven long-range elastic string, J. Stat. Mech. (2007) P01019.

[63] D. Ertaş and M. Kardar, Critical dynamics of contact line depinning, Phys. Rev. E **49**, R2532 (1994).

[64] P. Chauve, P. Le Doussal, and K. Jörg Wiese, Renormalization of Pinned Elastic Systems: How Does it Work Beyond One Loop?, Phys. Rev. Lett. **86**, 1785 (2001).

[65] J. Schmittbuhl and K. J. Måløy, Direct Observation of a Self-Affine Crack Propagation, Phys. Rev. Lett. **78**, 3888 (1997).

[66] K. T. Tallakstad, R. Toussaint, S. Santucci, J. Schmittbuhl, and K. J. Måløy, Local dynamics of a randomly pinned crack front during creep and forced propagation: An experimental study, Phys. Rev. E **83**, 046108 (2011).

[67] T. Vincent-Dospital, A. Cochard, S. Santucci, K. J. Måløy, and R. Toussaint, Thermally activated intermittent dynamics of creeping crack fronts along disordered interfaces, Sci. Rep. **11**, 20418 (2021).

[68] A. Prevost, E. Rolley, and C. Guthmann, Dynamics of a helium-4 meniscus on a strongly disordered cesium substrate, Phys. Rev. B **65**, 064517 (2002).

[69] M. A. Rubio, C. A. Edwards, A. Dougherty, and J. P. Gollub, Self-Affine Fractal Interfaces from Immiscible Displacement in Porous Media, Phys. Rev. Lett. **63**, 1685 (1989).

[70] P. M. Shearer, G. A. Prieto, and E. Hauksson, Comprehensive analysis of earthquake source spectra in southern California, J. Geophys. Res. **111** (2006).

[71] D. T. Trugman and P. M. Shearer, Application of an improved spectral decomposition method to examine earthquake source scaling in Southern California: Earthquake source scaling in Southern California, J. Geophys. Res. Solid Earth **122**, 2890 (2017).

[72] D. Houdoux, A. Amon, D. Marsan, J. Weiss, and J. Crassous, Micro-slips in an experimental granular shear band replicate the spatiotemporal characteristics of natural earthquakes, Commun. Earth Environ. **2**, 90 (2021).

[73] E. A. Jagla, F. P. Landes, and A. Rosso, Viscoelastic Effects in Avalanche Dynamics: A Key to Earthquake Statistics, Phys. Rev. Lett. **112**, 174301 (2014).

[74] T. W. J. de Geus, Supporting data: How collective asperity detachments nucleate slip at frictional interfaces, Zenodo (2019), doi:10.5281/zenodo.3477938.

[75] F. Barras, M. Aldam, T. Roch, E. A. Brener, E. Bouchbinder, and J.-F. Molinari, The emergence of crack-like behavior of frictional rupture: Edge singularity and energy balance, Earth Planet. Sci. Lett. **531**, 115978 (2020).